

Evidence for Radial Expansion at the Core of the Orion Complex with *Gaia* EDR3

CAMEREN SWIGGUM,¹ ELENA D'ONGHIA,¹ JOÃO ALVES,² JOSEFA GROßSCHEDL,² MICHAEL FOLEY,³ CATHERINE ZUCKER,³
STEFAN MEINGAST,² BOQUAN CHEN,⁴ AND ALYSSA GOODMAN³

¹*Department of Astronomy, University of Wisconsin, 475 North Charter Street, Madison, WI 53706, USA*

²*University of Vienna, Department of Astrophysics, Türkenschanzstraße 17, 1180 Vienna, Austria*

³*Center for Astrophysics | Harvard & Smithsonian, 60 Garden St., Cambridge, MA 02138, USA*

⁴*Sydney Institute for Astronomy, The University of Sydney, School of Physics A28, Camperdown, NSW 2006, Australia*

ABSTRACT

We present a phase-space study of two stellar groups located at the core of the Orion complex: Briceño-1 and Orion Belt Population-near (OBP-near). We identify the groups with the unsupervised clustering algorithm, Shared Nearest Neighbor (SNN), which previously identified twelve new stellar substructures in the Orion complex. For each of the two groups, we derive the 3D space motions of individual stars using *Gaia* EDR3 proper motions supplemented by radial velocities from *Gaia* DR2, APOGEE-2, and GALAH DR3. We present evidence for radial expansion of the two groups from a common center. Unlike previous work, our study suggests that evidence of stellar group expansion is confined only to OBP-near and Briceño-1 whereas the rest of the groups in the complex show more complicated motions. Interestingly, the stars in the two groups lie at the center of a dust shell, as revealed via an extant 3D dust map. The exact mechanism that produces such coherent motions remains unclear, while the observed radial expansion and dust shell suggest that massive stellar feedback could have influenced the star formation history of these groups.

Keywords: Star forming regions: individual (Orion Complex) – stars: kinematics; dynamics; ages

1. INTRODUCTION

The formation and evolution of star clusters is a complex process that depends crucially on the formation of the individual stars and how feedback mechanisms, including winds, radiation pressure, and supernovae, affect their environment. Young stars are usually grouped in clusters and are located within their natal star-forming regions. In contrast to younger stars, older stars are found dispersed throughout the Galactic field.

The role of gas in the formation and evolution of bound clusters or associations of stars is still poorly understood (e.g., Krause et al. 2020). A popular scenario posits that stars form and temporarily persist in dense molecular clouds, held together by the gravitational potential of the remaining gas (Lada & Lada 2003). The gas is eventually blown-out by feedback from stellar winds and supernovae events. Stars may disperse due to this gas expulsion and the associated change in gravitational potential (Hills 1980; Goodwin & Bastian

2006; Baumgardt & Kroupa 2007; Krause et al. 2020). Recent simulations also suggest that the expelled gas can flip a stellar association’s gravitational potential and elicit “gravitational feedback”, accelerating the expansion (e.g. Krause et al. 2020; Zamora-Avilés et al. 2019). Another model theorizes that once the gas is expelled, associations of stars might form by compression in the expanding shell (Elmegreen & Lada 1977).

The Orion complex is the most massive star-forming region in the solar vicinity (Bally 2008). Given its proximity (≈ 400 pc, Zucker et al. 2020; Großschedl et al. 2018), its mass ($> 10^5 M_{\odot}$; Lada et al. 2010), and the presence of multi-phase gas and stars at various evolutionary stages, Orion represents one of the best places to observe young stars in their natal environments.

Before the *Gaia* era, the classification of reliable associations and young clusters within the Orion complex was a challenge. While overdensities of stars were identified (e.g. Blaauw 1964; Brown et al. 1994; Bally 2008), often these overdensities appeared superimposed on the plane of the sky. The lack of accurate distances and proper motions prevented a separation of distinct groups

in true 3D space, making it difficult to classify the stellar associations in the Orion complex.

This situation has changed with the advent of the European Space Agency’s (ESA) *Gaia* Mission, which has provided distances and proper motions for tens of thousands of young stars in the vicinity of Orion (Gaia Collaboration et al. 2016). These data, supplemented by radial velocities (RVs) from *Gaia* and the Sloan Digital Sky Survey IV (SDSS-IV; Majewski et al. 2017) APOGEE-2 (Blanton et al. 2017), and GALAH DR3 (Buder et al. 2020), have allowed the use of clustering algorithms to identify the stellar associations in phase-space, with implications for understanding how young clusters form and evolve.

A recent study of the proper motions of stellar populations within the Orion Nebular Complex (ONC) reveals that this young star-forming region is bound, with little evidence of expansion (Kuhn et al. 2019). Other works explored the entire Orion complex and identified numerous stellar groups of various ages (e.g. Kubiak et al. 2017; Kounkel et al. 2018; Kos et al. 2019; Zari et al. 2019). A 6D phase-space analysis of the λ Orion region has shown evidence for expansion (Kounkel et al. 2018). Additionally, a gas study of Orion has also shown evidence for expansion likely due to strong stellar feedback (Großschedl et al. 2020).

Chen et al. (2020) applied an unsupervised clustering algorithm to *Gaia* DR2 data and identified 21 stellar groups in the Orion Complex. While nine of them overlap with stellar groups previously identified in the Orion region (Briceño et al. 2007; Alves & Bouy 2012; Kounkel et al. 2018), twelve were newly discovered. Recently, Kounkel et al. (2018) cataloged the Orion region groups using a different clustering algorithm. Kounkel (2020) further analyzed the groups’ phase space and claimed that the entire complex is expanding from a central region. Here we show that the expansion is most evident in two massive stellar groups in Orion, namely OBP-near and Briceño-1, which exhibit a “Hubble flow” like expansion pattern similar to those found in other star-forming regions (e.g. Wright & Mamajek 2018; Wright et al. 2019; Kuhn et al. 2019; Cantat-Gaudin et al. 2019; Román-Zúñiga et al. 2019). Our analysis uses *Gaia* EDR3, APOGEE-2, and GALAH DR3 to characterize the stars in the phase space and determine the age of the two groups of which OBP-near is newly discovered in a previous work (Chen et al. 2020).

In Section 2, we layout the data and methodology used to identify the stellar groups and study their dynamics and ages. Section 3 reports the main results of our study. Section 4 discusses physical scenarios that could lead to

our results and compare to previous works. Our results are briefly summarized in Section 5.

2. DATA ANALYSIS

2.1. SNN Stellar Groups

Chen et al. (2020) applied two clustering algorithms, namely Shared Nearest Neighbor (SNN; Chen et al. 2018) and *EnLink* (Sharma & Johnston 2009), to *Gaia* DR2 in the vicinity of Orion, to uncover stellar groups clustered in RA, DEC, parallaxes (α, δ, ϖ) and proper motions (μ_α, μ_δ). Advantages of this approach and its applied analysis include: 1) the ability to omit stars that unlikely belong to any group (unclassified stars); 2) the use of a density threshold criterion to balance the high and low-density regions in the 5D-space; 3) the assignment of group stability scores based on how many times the star appears in each of the total iterations (7,000 in Chen et al. 2020) and group membership probability.

Our study focuses on two groups labeled as SNN 1 and SNN 3 in Chen et al. (2020). SNN 1 is named “Briceño-1” due to its significant overlap with the 25 Orionis stellar population studied by Briceño et al. (2007).¹ The group is the most stable of all groups recovered in the original SNN analysis with a stability score of 3393 (out of 7,000). The plane-of-sky region of this stellar population is notably classified as the Ori OB1a sub-association and its average distance from the Sun is 350 pc. SNN 3 is named “OBP-near” and is newly discovered by the SNN clustering algorithm. It lies in the Ori OB1b sub-association (Blaauw 1964) in the plane of the sky. OBP-near has a stability score of 2847, making it the third most stable group discovered in the SNN analysis. Its average distance from the Sun is 360 pc, establishing itself at the front of the Orion Belt Population, hence the distinguishing title “near”.

Compared to *Gaia* DR2, EDR3 shows $\sim 30\%$ improvement in parallax precision and an improvement in proper motions by a factor of ~ 2 (Gaia Collaboration et al. 2020). We query the *Gaia* EDR3 database using the same region selection for Orion as used in Chen et al. (2020), specifically as $75^\circ < \alpha < 90^\circ$, $-15^\circ < \delta < 15^\circ$, $2 < \varpi < 5$ mas, $-4 < \mu_\alpha < 4$ mas/yr, and $-4 < \mu_\delta < 4$ mas/yr, with a cut of $\varpi/\sigma_\varpi > 5$, which yields 33,811 stars. We perform 500 iterations of SNN, each adopting a range of values for the free parameters n_{xyz} and d_{pm} . The n_{xyz} parameter defines the number of nearest neighbors in 3D Cartesian position-space computed for each star. The d_{pm} parameter is

¹ The prominent B star 25 Ori is not a member of SNN 1, hence the differing choice in the group’s name.

the maximum difference in proper motions between a star and its neighbors, computed for each star. We adopt uniform distributions of n_{xyz} and d_{pm} between 10–800 pc and 0–0.40 mas/yr, respectively. For the initial group finding, the parameters $min_samples$ and eps are fixed to the values in $eps=0.5$ and $min_samples=20$. This choice selects candidates with at least 20 stars having more than 50% shared nearest neighbors. We set $eps=0.7$ and the minimum number of retrieved groups, $min_samples$, is set to 15 (see Chen et al. (2020) for details). We adopt a probability cut of 2%, meaning a star was included in a given group for at least 10 out of 500 iterations, greatly reducing the number of overlapped members. The average probability is 16% after this cut.

Using EDR3, we retrieve Briceño-1 and OBP-near, along with the other SNN groups. Around 80% of the original Briceño-1 stars are part of the group with 306 new stars. Around 52% of the original OBP-near stars belong to the group with an additional 252 new stars. Most of the stars that are no longer members of the groups are reclassified as field stars. *Gaia* EDR3 average position and velocities of both groups are provided in Table 1.

2.2. Radial Velocities

To study the 3D kinematics of both OBP-near and Briceño-1, we require radial velocity (RV) measurements. We first cross-match the stars from OBP-near and Briceño-1 with the Sloan Digital Sky Survey IV (SDSS-IV; Majewski et al. 2017) APOGEE-2 (Blanton et al. 2017) adopting SYNTHVELIO_AVG² as the RV measurement and SYNTHVERR as their corresponding errors. Additionally, we include more RVs by cross-matching the two groups to GALAH DR3 (Buder et al. 2020). When a star has RV measurements in multiple surveys, we adopt the RV with the highest S/N, leading to a preference for APOGEE-2 RVs, followed by GALAH DR3, and then *Gaia* DR2. There is no apparent systematic shift between APOGEE-2 and *Gaia* DR2 RVs, however there is a positive shift in GALAH DR3 RVs by ~ 0.7 km s⁻¹ when comparing to APOGEE-2. We subtract this value from GALAH DR3 RVs to be inline with the *Gaia* and APOGEE-2 RVs.

There is a large spread in the RV distribution, likely due to spectroscopic binaries in the sample. A CMD inspection of the groups’ stars with discrepant RVs reveals that many are O and B-type stars. According to Chini et al. (2012), the binary rate for stars with mass $> 16 M_{\odot}$ is $\sim 80\%$ and drops to $\sim 20\%$ for stars with

mass $\sim 3 M_{\odot}$. We exclude these stars by restricting the RVs to the range $17 < RV < 26$ km s⁻¹. Overall, a total of 221 stars with accurate RVs remain in the sample of both groups.

2.3. Positions and Kinematics

Knowing the positions and velocities of the two groups, we can constrain their dynamical evolution. We convert parallax to distance using $d = 1/\varpi$. We adopt the Astropy python package (Astropy Collaboration et al. 2018) and convert the sky coordinates, distances, proper motions, and radial velocities of both groups’ stars to 3D Galactic cartesian coordinates (X, Y, Z) pc and Heliocentric velocity components to (U, V, W) km s⁻¹. A correction is made to the solar motion by subtracting $(U, V, W)_{\odot} = (11.1, 12.24, 7.25)$ km s⁻¹ from the stars’ velocities (Schönrich et al. 2010) to obtain (u, v, w) velocities with respect to the LSR. We also subtract Galactic rotation values at each star’s Galactocentric radius using the MilkyWay2014 potential from the Galpy python package (Bovy 2015). The difference in galactic rotation across the two groups is modest (~ 0.006 km s⁻¹ pc⁻¹). A correction to the proper motions’ perspective contraction is made using Equation 13 from van Leeuwen (2009).

Errors on the positions and velocities are estimated using a Monte Carlo approach. The astrometric and RV errors are assumed to be normally distributed and uncorrelated given the proximity of Orion and the region’s data quality. For a given star, Gaussian distributions are created for each measurement with the input errors corresponding to the distributions’ standard deviations and the observed values corresponding to the mean. These distributions are sampled in parallel 10,000 times and transformed from spherical to Heliocentric Galactic cartesian coordinates. The standard deviations of each dimension’s resulting distribution are then calculated and stored as their corresponding errors.

Finally, we define our study’s reference frame by subtracting the median (u, v, w) motions from the combined groups and adopting the notation (X, Y, Z, v_x, v_y, v_z) .

2.4. Age Estimates

To estimate the ages of Briceño-1 and OBP-near, we fit isochrones to the groups’ CMDs using their *Gaia* EDR3 photometry. We use the latest PARSEC³ isochrones with the updated EDR3 passband definitions (Marigo et al. 2017). Similar to previous we consider both a stellar population’s age (t) and extinction (A_V) as free parameters when fitting the models with an age

² An average of the RV measurements from cross-correlating to the best-fit synthetic spectrum.

³ <http://stev.oapd.inaf.it/cgi-bin/cmd>

Table 1. Summary of Groups

Group Name	$\bar{\alpha}$	$\bar{\delta}$	\bar{d}	$\bar{\mu}_\alpha$	μ_δ	$\bar{R}V$	N	N _{RV} (A-2)	N _{RV} (GDR3)	N _{RV} (<i>Gaia</i>)
	(deg)	(deg)	(pc)	(mas/yr)	(mas/yr)	(km/s)				
(1)	(2)	(3)	(4)	(5)	(6)	(7)	(8)	(9)	(10)	(11)
Briceño-1	81.8 (0.9)	2.3 (1.1)	346 (11)	1.4 (0.2)	−0.3 (0.3)	21.2 (1.5)	892	71	26	5
OBP-near	83.8 (1.2)	−1.6 (0.9)	357 (14)	1.6 (0.3)	−1.3 (0.2)	22.2 (1.9)	655	105	7	7

NOTE—The two stellar groups as identified with the SNN clustering algorithm: Briceño-1 and OBP-near. In column (1) we give the name of the group; (2) average/ 1σ spread in RA; (3) average/ 1σ spread in DEC; (4) average/ 1σ spread in distance; (5) average/ 1σ spread in PMRA; (6) average/ 1σ spread in PMDEC; (7) average/ 1σ spread in heliocentric radial velocity; (8) number of stars in each group; (9) number of APOGEE-2 radial velocities used; (10) we number GALAH DR3 radial velocities used; (11) number of *Gaia* DR2 radial velocities used.

range of $1 < t < 20$ Myr and a step size of 0.05 Myr and an extinction range of $0.0 < A_V < 1.0$ mag with a step size of 0.1 mag (Zari et al. 2019). For simplicity, we assume a solar metal fraction of $Z = 0.0158$.

The isochrone fitting method follows a standard maximum log-likelihood estimation procedure. Assuming the errors are Gaussian, we measure the likelihood of a star with a given mass, m , to come from an isochrone with parameters, $\theta = (t, A_V)$ as:

$$\ln(L(\theta, m)) = \sum_{i=1}^n \ln\left(\frac{1}{(2\pi)^{1/2}\sigma_i}\right) - \frac{\chi^2}{2} \quad (1)$$

where:

$$\chi^2 = \sum_{i=1}^n \left(\frac{M_{g_i}^{\text{obs}} - M_{g_i}(\theta, m)}{\sigma_i}\right)^2 \quad (2)$$

A quality cut is applied to the *Gaia* photometry following `phot_g_mean_flux_over_error` > 20 and `phot_rp_mean_flux_over_error` > 20. We interpolate the isochrones to match the stars’ *Gaia* $G - G_{RP}$ color. M_{g_i} is the absolute magnitude calculated from the G band photometry and parallax. $M_{g_i}(t, m)$ is the absolute magnitude of the interpolated isochrone point corresponding to the same color as the observed star. The best-fit age (hereafter t_{iso}) is found by maximizing Eq. 1 (minimizing Eq. 2) where the summation is performed across all CMD points of the group. Age uncertainties are determined by finding the range of ages with corresponding likelihoods within 1σ of the maximum likelihood. These statistical uncertainties do not consider the biases that contribute to isochrone fitting: unresolved binaries, model uncertainties, and differential extinction. An unresolved binary sequence is apparent in both groups and is likely biasing the ages towards younger values.

3. RESULTS

When viewed in three spatial dimensions, the positions and kinematics reveal that the two groups are expanding radially away from a common center (Figure 1). Figure 2 shows a correlation between the position and velocity for both stellar groups. The slopes of the linear fits to the position-velocity profiles are $(\kappa_x, \kappa_y, \kappa_z) = (0.114 \pm 0.009, 0.122 \pm 0.003, 0.126 \pm 0.005)$ km s^{−1} pc^{−1}. Hence, stars further away from the groups’ center are moving faster. A fit to the stars’ speeds as a function of radius yields a slope of $\kappa_r = 0.101 \pm 0.007$ km s^{−1} pc^{−1} when the center is estimated by-eye to be $X = -310, Y = -133, Z = -105$ pc. This center is chosen as opposed to a center calculated using the average stellar position due to the non-uniform spatial distribution of stars when considering the two groups’ combined profile. The stars’ average speed is 2.45 ± 0.03 km s^{−1} and the velocity dispersion of both groups is ~ 0.80 km s^{−1}.

These linear profiles show evidence for ballistic expansion, where the highest velocity stars have had sufficient time to travel further outwards from the center. A process where stars are accelerated outwards due to violent changes in the region’s gravitational potential may also play a roll in creating the observed expansion profile (Zamora-Avilés et al. 2019).

The correlation is tighter in $y - v_y$ and $z - v_z$ than in $x - v_x$. A Kendall’s τ correlation test yields $\tau_{x-v_x} = .20$, $\tau_{y-v_y} = .73$, and $\tau_{z-v_z} = .50$, each with a statistical significance of $p < 1 \times 10^{-5}$. We note that among the three directions, the x-axis is the most aligned with the line-of-sight direction. As illustrated in Figure 2, this bias results with large uncertainties in the parallaxes and RV estimates for the correlation projected along this component.

The expansion time estimate can be inferred using the stars’ velocities as a function of position. For each of the position-velocity slopes found in Figure 2 we calculate the expansion time, $t_{\text{exp}} = 1/\gamma\kappa$, where $\gamma = 1.0227$

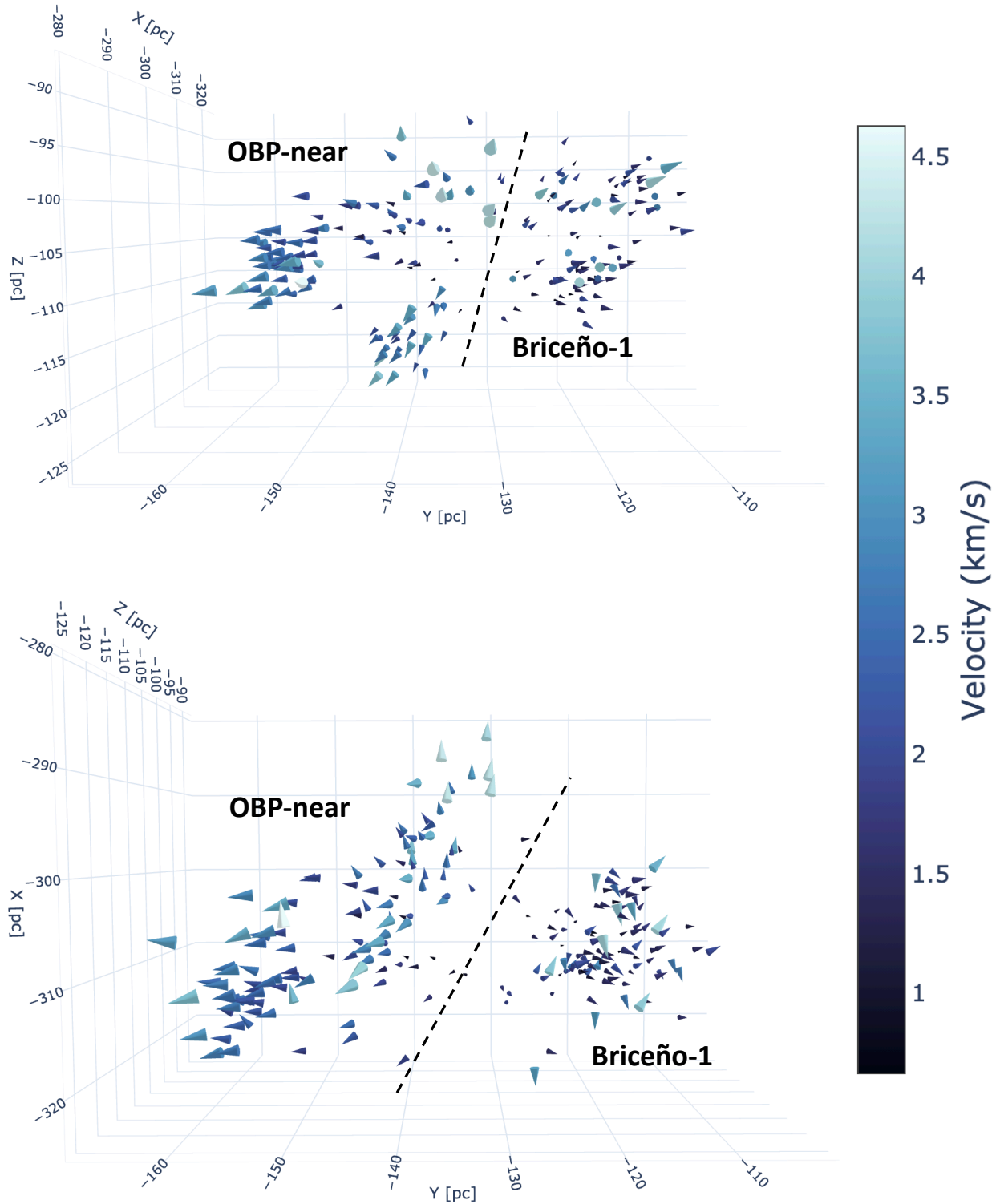


Figure 1. 3D kinematics of stars with available RVs in OBP-near and Briceño-1 in Heliocentric Galactic cartesian coordinates after subtracting the combined average of their kinematics in each dimension. Larger, lighter-colored cones represent faster-moving stars, and smaller, darker-colored cones represent slower-moving stars. The directions of the cones' apices represent the directions of the stars' motions. The dashed line in each panel marks the spatial division of the two groups from that viewing angle. An interactive version is available [here](#), or in the online version of the published article.

pc Myr⁻¹ km⁻¹ s. We find $t_{\text{exp},x} = 8.58$ Myr, $t_{\text{exp},y} = 8.00$ Myr, $t_{\text{exp},z} = 7.72$ Myr, and $t_{\text{exp},r} = 9.68$ Myr. When tracing the stars' positions back in time (assuming constant velocity), we find that the groups were most compact around 7.5 Myr ago, with a distance of only 6 pc between the two groups' respective centers.

Figure 3 shows the color-magnitude diagram (CMD) of Briceño-1 and OBP-near with their best-fit isochrone values, t_{iso} , and their associated uncertainties. From these isochrones, both groups are found to have an extinction of $A_V = 0.2$ mag. Briceño-1 appears to be ~ 3 Myr older than OBP-near based on its t_{iso} value and its offset on the CMD. However, the strong main-sequence overlap between the two groups makes this offset subtle. Note again that the t_{iso} values are likely lower limits due to the bias from unresolved binaries in the sample. Additionally, Briceño-1 is positioned along the LOS, directly in front of the 20 Myr old group, ASCC20 (Kos et al. 2019, SNN7 in Chen et al. 2020), possibly biasing the isochrone fit for Briceño-1 towards an older value. However, SNN results do not indicate significant overlap from ASCC20. An investigation into the infrared colors of both groups' stars is presented in Appendix A and points towards OBP-near indeed having a slightly younger age than Briceño-1.

4. DISCUSSION

A recent study performed a hierarchical clustering analysis on Orion and claimed that the entire complex shows clear radial expansion from a central region due to a SNe explosion (Kounkel et al. 2018; Kounkel 2020). These studies recovered 190 individual groups, which were then recombined into larger groups as Orion A, B, C, D, and λ Orion. Orion D was reported to consist of stars associated with the Orion OBlab region and more diffuse populations just outside of it. We apply the SNN clustering algorithm to the region and find that 43% (594 stars) of OBP-near and Briceño-1 stars can be cross-matched to Orion D of Kounkel et al. (2018). Other groups recovered in Chen et al. (2020) including ASCC20 (SNN 7; Kos et al. 2019), L1616 (SNN 8), and Orion X (SNN 20; Bouy & Alves 2015) partially cross-match to Orion D as well. Additionally, 50% of stars from OBP-d (SNN 6; Kubiak et al. 2017), OBP-b (SNN 9; Kubiak et al. 2017), ome Ori (SNN 14; Chen et al. 2020), OBP-West (SNN 16; Chen et al. 2020), and OBP-far (SNN 19; Chen et al. 2020) overlap with Orion C.

It was claimed that Orion D shows signs of expansion by analyzing proper motions with Gaia DR2 (Kounkel et al. 2018); however, Orion D contains a mix of smaller groups that differ in age and kinematics. Isochrone fits

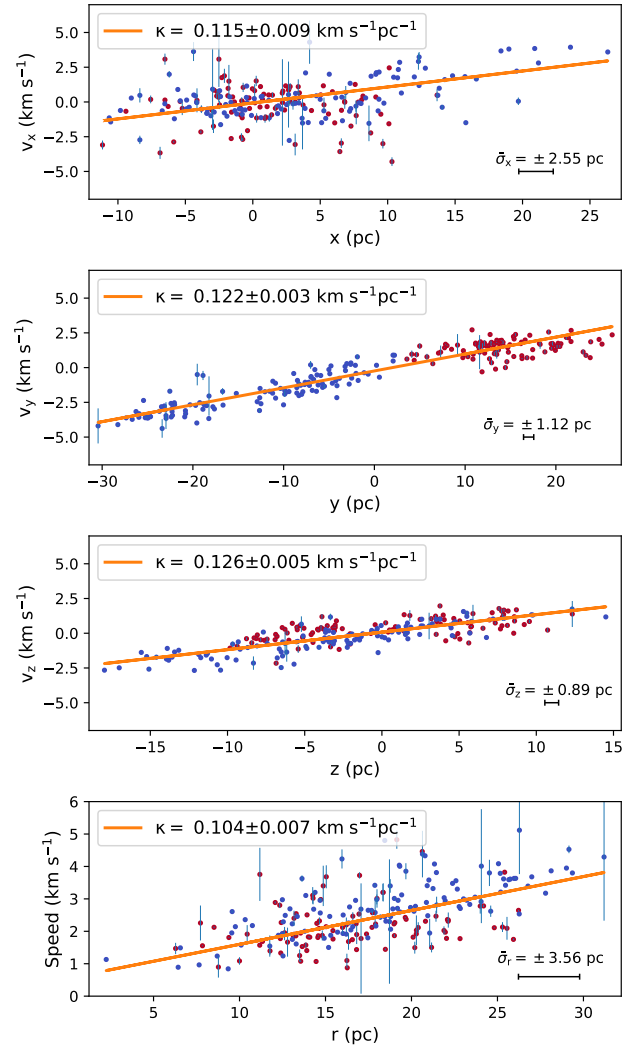


Figure 2. Position-velocity profiles of stars in the combined reference frame of OBP-near (blue points) and Briceño-1 (red points). Each panel shows the position-velocity profile for a given Cartesian component. Regression lines (orange) are fit to the combined profiles of OBP-near and Briceño-1 in order to estimate the expansion slope, κ , which is quoted in the legends. Individual velocity errors are displayed and the mean of the position errors is shown in the lower right-hand corner of each panel.

to each of the SNN groups in this region indicate an age range between 6 and 20 Myr, with the oldest being ASCC20. These values suggest that Orion D has multiple stellar populations which presumably did not form together.

Furthermore, previous work placed all of these groups in a single, common reference frame and proposed that the entire complex is currently expanding from a central region due to a supernova event that occurred 6 Myr ago (Kounkel 2020). As part of the proposal, Orion

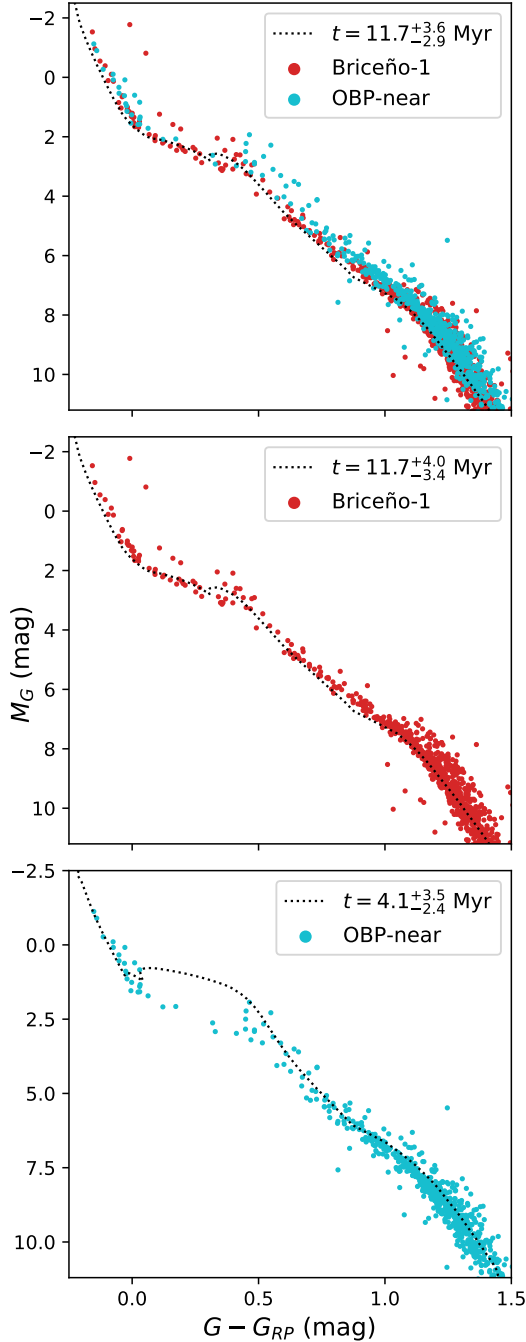


Figure 3. The CMDs of OBP-near (cyan dots) and Briceño-1 (red dots) stars: the top panel shows the combined CMD of both groups with their combined best-fit isochrone (dotted line); the middle panel shows the CMD of Briceño-1 and its best-fit isochrone; the bottom panel shows the CMD of OBP-near and its best-fit isochrone. The legend in each panel quotes the associated age of the isochrone fit and its uncertainty.

C and D were once part of the same molecular cloud, split by the supernova explosion that separated them

into two distinct regions. To test the hypothesis we extend the analysis of OBP-near and Briceño-1 to the rest of the SNN groups. While most of the original groups are re-derived in Section 2, here we utilize the original catalog from Chen et al. (2020) (except OBP-near and Briceño-1) as their study more carefully considers the entire Orion complex. We update the astrometry of these SNN groups by cross-matching to *Gaia* eDR3. SNN 13, 18, 22, and 25 are discarded, as Chen et al. (2020) finds them to strongly overlap with some of the larger identified groups.

We follow the SNN groups’ motion in a common reference frame backwards/forwards in time ± 8 Myr (see Figure 4) and find that OBP-near and Briceño-1 are the only groups that clearly trace back to a common center. Two smaller SNN groups, L1616 ($N=146$ stars) and Orion X ($N=135$ stars), may be part of the expansion. Großschedl et al. (2020) analyzes the complex’s gas dynamics and finds L1616 to be part of an expanding region, however the stars they study are younger and might not match the stars of L1616 from Chen et al. (2020). While the velocities of L1616’s stars from SNN are a factor of ~ 3 too small to be consistent with the expansion profile of OBP-near and Briceño-1 (Figure 2), this may be due to L1616 having a greater distance from the source of feedback during its onset. NGC 1980 partially overlaps with the Orion A region of Kounkel et al. (2018). However, our analysis shows that it does not originate from the expansion center when followed back in time. It’s direction of motion does elicit the possibility that it has formed from the onset of triggered star formation due to feedback as originally proposed in Kounkel (2020) and Großschedl et al. (2020). Note that there is an open debate questioning whether NGC 1980 is a separate, foreground population to the ONC group reported in Kounkel et al. (2018) (see Alves & Bouy 2012 and Fang et al. 2017 for further discussion).

The SNN analysis shows that groups with similar ages as Orion C and the ~ 20 Myr old groups overlapping with Orion D are moving through the complex rather than expanding from Orion’s core. Hence, signs of expansion are most evident in OBP-near and Briceño-1 while the other groups show a more complex dynamical history.

The radial expansion shown by OBP-near and Briceño-1 groups may be related to past SNe explosions or strong stellar winds which might have occurred at the core of Orion. Such winds and SNe would be expected to create cavities in the interstellar medium, manifesting as shells and bubbles (see e.g. Smith et al. 2020; Kim & Ostriker 2018). Figure 5 shows the spatial location of OBP-near and Briceño-1 (colored dots), as compared

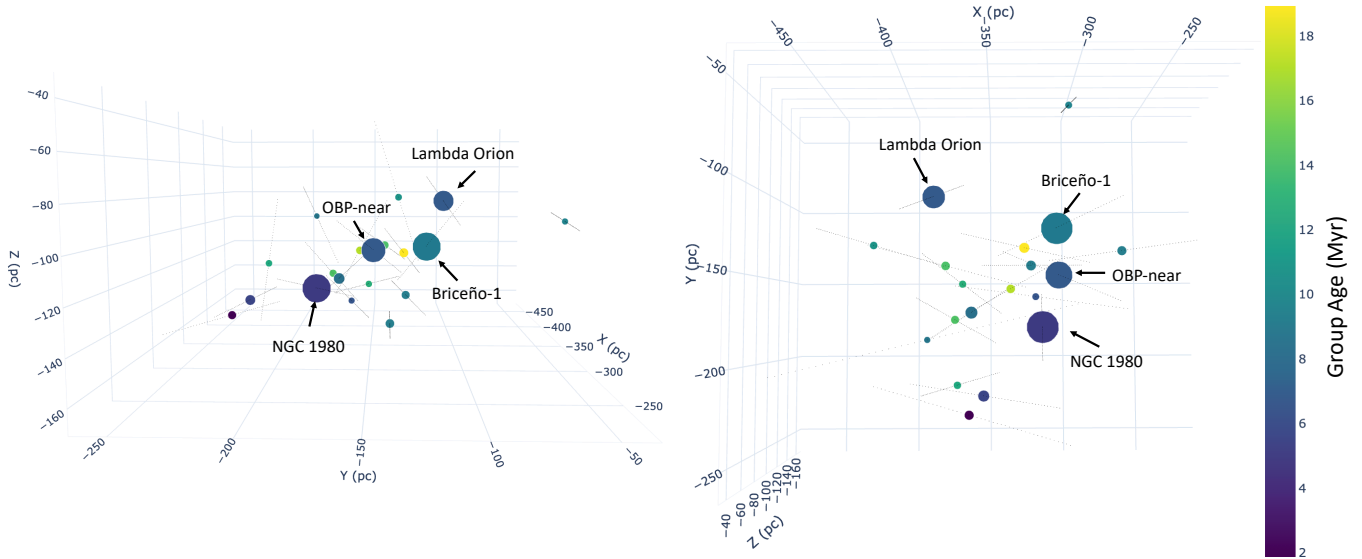


Figure 4. Interactive animation tracing the evolution of the SNN groups (Chen et al. 2020) (colored dots) forwards (+8 Myr) and backwards (−8 Myr) in time in the Orion reference frame assuming a constant speed. Thin, dotted lines show the trace of each group’s motion. Each panel in the static version shows a different view point of the groups’ present-day positions. Groups are colored by their ages as measured from isochrone fits and their sizes indicate the number of stars they contain. Throughout the animation, filled dots become open dots if the chosen time is prior to a group’s formation time. The four most massive groups are indicated by the arrows and labels. Moving the time slider left moves the groups back in time and to the right moves them forwards in time. The interactive animation can be found [here](#), or in the online version of the published article.

to a high-resolution 3D spatial map of the nearby interstellar medium derived from 3D dust mapping (Leike et al. 2020). OBP-near and Briceño-1 lie at the center of a dust shell, which would indicate that past feedback events occurred within the two groups. Evidence of a dust shell is also seen in a complementary 3D dust map of the Orion A region, with the nearest part of the dust shell coincident with a previously undiscovered foreground cloud at a distance between $\approx 315 - 345$ pc (see Figure 6 in Rezaei Kh. et al. 2020). Past studies have also found evidence for an expanding H I shell that roughly surrounds the two groups’ plane-of-sky positions but with a center more aligned with OBP-near (Chromey et al. 1989; Ochsendorf et al. 2015).

One possible scenario to explain our observations suggests that stars which today identify as OBP-near and Briceño-1 formed approximately at the same time as one bound cluster at the core. A major feedback event dispersed the gas in the original molecular cloud after the stars formed. While the violent change of the gravitational potential might unbind the system and lead the stars to expand, it is unclear whether this mechanism can drive the stars into a ballistic expansion with the symmetry displayed in Figure 1. As stated previously, rapid changes to the potential following gas/dust dispersal could aid in accelerating the stars (Zamora-Avilés et al. 2019).

Another theory posits that star associations may form in gas compressed layers of the expanding shell from shock fronts after SN events or other massive stellar feedback. In this scenario, the grouped stars will move at the same velocity as the expanding gas shell they formed in (Elmegreen & Lada 1977). Yet, it is unclear whether this process will lead to the expansion with the properties observed in Figure 1. Such a scenario, where star formation is triggered sequentially, could explain an intrinsic age difference between OBP-near and Briceño-1; if feedback took place closer to one side of the progenitor cloud, then the onset of star formation could have occurred at different times across different locations of the expanding gas shell.

5. CONCLUSIONS

The astrometric measurements of the *Gaia* mission provided in DR2 and EDR3, supplemented by APOGEE-2 and GALAH DR3, have enabled a systematic study of the 3D kinematics of OBP-near and Briceño-1, two stellar groups at the core of the Orion complex. This work shows direct evidence of ballistic expansion occurring locally at the core of the Orion complex. While previous works found some evidence of coherent motions in the Orion complex, this study shows compelling evidence of stellar expansion in a massive star-forming region. The stars are currently located at the center of a dust shell, suggesting that their expan-

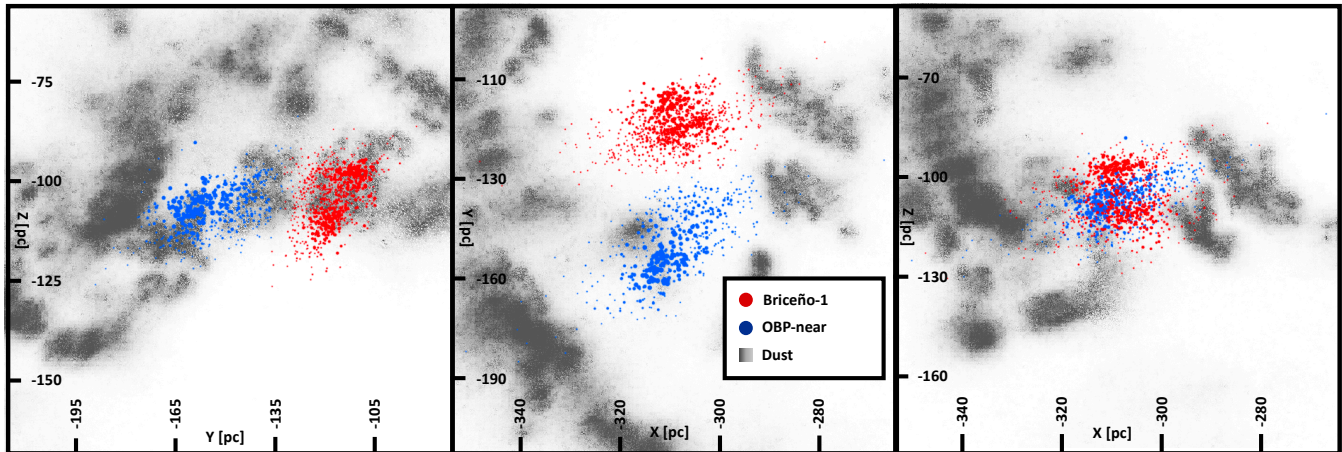


Figure 5. The spatial location of OBP-near and Briceño-1, overlaid on a 3D spatial map of interstellar dust (Leike et al. 2020). As apparent in the top down X-Y view (middle panel), the OBP and Briceño-1 groups lie at the center of a dust shell. The stars’ sizes indicate their probability to be group members assigned by SNN. An interactive version of this figure is available [here](#) or in the online version of the published article.

sion links to stellar feedback events. However, the process driving the relatively symmetric radial expansion shown in this study remains unclear. Upcoming work (Foley et al. in prep) will present further evidence for the connection between this radial expansion and stellar feedback. Future *Gaia* data releases are anticipated to significantly improve the astrometry of stars, which will allow for more accurate kinematic analyses of the entire Orion complex. Forthcoming observations and numerical studies of the interstellar medium will also help shed light on the relationship between feedback events and stellar dynamics

6. ACKNOWLEDGMENTS

The authors are grateful to B. Elmegreen and J. Gallagher for insightful suggestions. This work has made use of data from the European Space Agency (ESA) mission *Gaia* (<https://www.cosmos.esa.int/gaia>), processed by the *Gaia* Data Processing and Analysis Consortium (DPAC; <https://www.cosmos.esa.int/web/gaia/dpac/consortium>). Funding for the DPAC has been provided by national institutions, in particular the institutions participating in the *Gaia* Multilateral Agreement. This project was developed in part at the 2019 Santa Barbara *Gaia* Sprint, hosted by the Kavli Institute for Theoretical Physics at the University of California, Santa Barbara, and by the 2020 EDR3 Unboxing *Gaia* Sprint, hosted by the Center for Computational Astrophysics of the Flatiron Institute in New York City.

Funding for the Sloan Digital Sky Survey IV has been provided by the Alfred P. Sloan Foundation, the U.S. Department of Energy Office of Science, and the Participating Institutions. SDSS-IV acknowledges support and

resources from the Center for High Performance Computing at the University of Utah. The SDSS website is www.sdss.org.

SDSS-IV is managed by the Astrophysical Research Consortium for the Participating Institutions of the SDSS Collaboration including the Brazilian Participation Group, the Carnegie Institution for Science, Carnegie Mellon University, Center for Astrophysics — Harvard & Smithsonian, the Chilean Participation Group, the French Participation Group, Instituto de Astrofísica de Canarias, The Johns Hopkins University, Kavli Institute for the Physics and Mathematics of the Universe (IPMU) / University of Tokyo, the Korean Participation Group, Lawrence Berkeley National Laboratory, Leibniz Institut für Astrophysik Potsdam (AIP), Max-Planck-Institut für Astronomie (MPIA Heidelberg), Max-Planck-Institut für Astrophysik (MPA Garching), Max-Planck-Institut für Extraterrestrische Physik (MPE), National Astronomical Observatories of China, New Mexico State University, New York University, University of Notre Dame, Observatório Nacional / MCTI, The Ohio State University, Pennsylvania State University, Shanghai Astronomical Observatory, United Kingdom Participation Group, Universidad Nacional Autónoma de México, University of Arizona, University of Colorado Boulder, University of Oxford, University of Portsmouth, University of Utah, University of Virginia, University of Washington, University of Wisconsin, Vanderbilt University, and Yale University.

Software: Astropy (Astropy Collaboration et al. 2018), NumPy (van der Walt et al. 2011), Plotly, Matplotlib (Hunter 2007), Glue (Robitaille et al. 2017), and Galpy (Bovy 2015).

REFERENCES

- Alves, J. & Bouy, H. 2012, *A&A*, 547, A97.
doi:10.1051/0004-6361/201220119
- Alves, J., Zucker, C., Goodman, A. A., et al. 2020, *Nature*, 578, 237
- Astropy Collaboration, Price-Whelan, A. M., Sipőcz, B. M., et al. 2018, *AJ*, 156, 123. doi:10.3847/1538-3881/aabc4f
- Bally, J. 2008, *Handbook of Star Forming Regions*, Volume I, 459
- Baumgardt, H. & Kroupa, P. 2007, *MNRAS*, 380, 1589.
doi:10.1111/j.1365-2966.2007.12209.x
- Bessell, M. S. & Brett, J. M. 1988, *PASP*, 100, 1134.
doi:10.1086/132281
- Blanton, M. R., Bershad, M. A., Abolfathi, B., et al. 2017, *AJ*, 154, 28
- Blaauw, A. 1964, *ARA&A*, 2, 213
- Bouy, H. & Alves, J. 2015, *A&A*, 584, A26.
doi:10.1051/0004-6361/201527058
- Bovy, J. 2015, *ApJS*, 216, 29
- Briceño, C., Hartmann, L., Hernández, J., et al. 2007, *ApJ*, 661, 1119
- Brown, A. G. A., de Geus, E. J., & de Zeeuw, P. T. 1994, *A&A*, 289, 101
- Buder, S., Sharma, S., Kos, J., et al. 2020, arXiv:2011.02505
- Cantat-Gaudin, T., Jordi, C., Wright, N. J., et al. 2019, *A&A*, 626, A17. doi:10.1051/0004-6361/201834957
- Chen, B., D’Onghia, E., Pardy, S. A., et al. 2018, *ApJ*, 860, 70. doi:10.3847/1538-4357/aac325
- Chen, B., D’Onghia, E., Alves, J., et al. 2020, *A&A*, 643, A114. doi:10.1051/0004-6361/201935955
- Chini, R., Hoffmeister, V. H., Nasser, A., et al. 2012, *MNRAS*, 424, 1925. doi:10.1111/j.1365-2966.2012.21317.x
- Chromey, F. R., Elmegreen, B. G., & Elmegreen, D. M. 1989, *AJ*, 98, 2203. doi:10.1086/115289
- Cropper, M., Katz, D., Sartoretti, P., et al. 2018, *A&A*, 616, A5
- Cutri, R. M., Wright, E. L., Conrow, T., et al. 2013, Explanatory Supplement to the AllWISE Data Release Products, by R. M. Cutri et al.
- Elmegreen, B. G. & Lada, C. J. 1977, *ApJ*, 214, 725.
doi:10.1086/155302
- Fang, M., Kim, J. S., Pascucci, I., et al. 2017, *AJ*, 153, 188.
doi:10.3847/1538-3881/aa647b
- Gaia Collaboration, Prusti, T., de Bruijne, J. H. J., et al. 2016, *A&A*, 595, A1. doi:10.1051/0004-6361/201629272
- Gaia Collaboration, Brown, A. G. A., Vallenari, A., et al. 2018, *A&A*, 616, A1
- Gaia Collaboration, Brown, A. G. A., Vallenari, A., et al. 2020, arXiv:2012.01533
- Geen, S., Watson, S. K., Rosdahl, J., et al. 2018, *MNRAS*, 481, 2548. doi:10.1093/mnras/sty2439
- Goodwin, S. P. & Bastian, N. 2006, *MNRAS*, 373, 752.
doi:10.1111/j.1365-2966.2006.11078.x
- Großschedl, J. E., Alves, J., Meingast, S., et al. 2018, *A&A*, 619, A106. doi:10.1051/0004-6361/201833901
- Großschedl, J. E., Alves, J., Teixeira, P. S., et al. 2019, *A&A*, 622, A149. doi:10.1051/0004-6361/201832577
- Großschedl, J. E., Alves, J., Meingast, S., et al. 2020, arXiv:2007.07254
- Hills, J. G. 1980, *ApJ*, 235, 986. doi:10.1086/157703
- Hunter, J. D. 2007, *Computing in Science and Engineering*, 9, 90. doi:10.1109/MCSE.2007.55
- Kim, C.-G. & Ostriker, E. C. 2018, *ApJ*, 853, 173.
doi:10.3847/1538-4357/aaa5ff
- Koenig, X. P. & Leisawitz, D. T. 2014, *ApJ*, 791, 131.
doi:10.1088/0004-637X/791/2/131
- Kos, J., Bland-Hawthorn, J., Asplund, M., et al. 2019, *A&A*, 631, A166. doi:10.1051/0004-6361/201834710
- Kounkel, M., Covey, K., Suárez, G., et al. 2018, *AJ*, 156, 84. doi:10.3847/1538-3881/aad1f1
- Kounkel, M. 2020, *ApJ*, 902, 122.
doi:10.3847/1538-4357/abb6e8
- Krause, M. G. H., Offner, S. S. R., Charbonnel, C., et al. 2020, *SSRv*, 216, 64. doi:10.1007/s11214-020-00689-4
- Kubiak, K., Alves, J., Bouy, H., et al. 2017, *A&A*, 598, A124
- Kuhn, M. A., Hillenbrand, L. A., Sills, A., et al. 2019, *ApJ*, 870, 32. doi:10.3847/1538-4357/aaef8c
- Kuhn, M. A., Hillenbrand, L. A., Carpenter, J. M., et al. 2020, *ApJ*, 899, 128. doi:10.3847/1538-4357/aba19a
- Lada, C. J. 1987, *Star Forming Regions*, 115, 1
- Lada, C. J. & Lada, E. A. 2003, *ARA&A*, 41, 57.
doi:10.1146/annurev.astro.41.011802.094844
- Lada, C. J., Muench, A. A., Luhman, K. L., et al. 2006, *AJ*, 131, 1574. doi:10.1086/499808
- Lada, C. J., Lombardi, M., & Alves, J. F. 2010, *ApJ*, 724, 687. doi:10.1088/0004-637X/724/1/687
- Leike, R. H., Glatzle, M., & Enßlin, T. A. 2020, *A&A*, 639, A138. doi:10.1051/0004-6361/202038169
- Luri, X., Brown, A. G. A., Sarro, L. M., et al. 2018, *A&A*, 616, A9
- Majewski, S. R., Schiavon, R. P., Frinchaboy, P. M., et al. 2017, *AJ*, 154, 94
- Marigo, P., Girardi, L., Bressan, A., et al. 2017, *ApJ*, 835, 77
- Ochsendorf, B. B., Brown, A. G. A., Bally, J., et al. 2015, *ApJ*, 808, 111. doi:10.1088/0004-637X/808/2/111

- Rezaei Kh., S., Bailer-Jones, C. A. L., Soler, J. D., et al. 2020, *A&A*, 643, A151. doi:10.1051/0004-6361/202038708
- Robitaille, T., Beaumont, C., Qian, P., et al. 2017, Zenodo
- Román-Zúñiga, C. G., Roman-Lopes, A., Tapia, M., et al. 2019, *ApJL*, 871, L12. doi:10.3847/2041-8213/aafb06
- Schönrich, R., Binney, J., & Dehnen, W. 2010, *MNRAS*, 403, 1829
- Sharma, S. & Johnston, K. V. 2009, *ApJ*, 703, 1061. doi:10.1088/0004-637X/703/1/1061
- Skrutskie, M. F., Cutri, R. M., Stiening, R., et al. 2006, *AJ*, 131, 1163. doi:10.1086/498708
- Smith, R. J., Treß, R. G., Sormani, M. C., et al. 2020, *MNRAS*, 492, 1594. doi:10.1093/mnras/stz3328
- Ward, J. L. & Kruijssen, J. M. D. 2018, *MNRAS*, 475, 5659. doi:10.1093/mnras/sty117
- Ward, J. L., Kruijssen, J. M. D., & Rix, H.-W. 2020, *MNRAS*, 495, 663. doi:10.1093/mnras/staa1056
- Wright, N. J. & Mamajek, E. E. 2018, *MNRAS*, 476, 381. doi:10.1093/mnras/sty207
- Wright, N. J., Jeffries, R. D., Jackson, R. J., et al. 2019, *MNRAS*, 486, 2477. doi:10.1093/mnras/stz870
- van der Walt, S., Colbert, S. C., & Varoquaux, G. 2011, *Computing in Science and Engineering*, 13, 22. doi:10.1109/MCSE.2011.37
- van Leeuwen, F. 2009, *A&A*, 497, 209. doi:10.1051/0004-6361/200811382
- Zamora-Avilés, M., Ballesteros-Paredes, J., Hernández, J., et al. 2019, *MNRAS*, 488, 3406. doi:10.1093/mnras/stz1897
- Zari, E., Brown, A. G. A., de Bruijne, J., et al. 2017, *A&A*, 608, A148. doi:10.1051/0004-6361/201731309
- Zari, E., Brown, A. G. A., & de Zeeuw, P. T. 2019, *A&A*, 628, A123
- Zucker, C., Speagle, J. S., Schlafly, E. F., et al. 2020, *A&A*, 633, A51. doi:10.1051/0004-6361/201936145

APPENDIX

A. INFRARED COLORS OF OBP-NEAR AND BRICEÑO-1

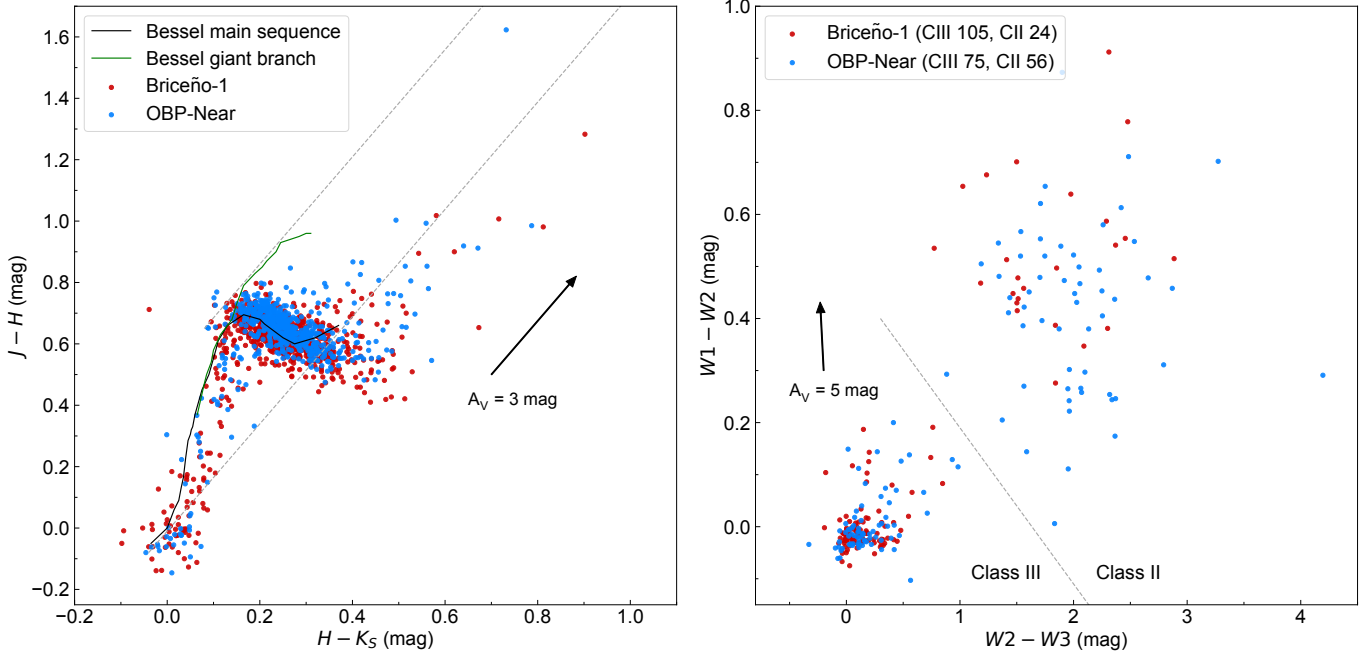


Figure 6. Infrared color-color diagrams for stellar members in Briceño-1 (red) and OBP-near (blue). *Left:* 2MASS near-infrared JHKs color-color diagram. Overplotted are the main sequence (black curve) and giant branch (green curve) from [Bessell & Brett \(1988\)](#) for reference. An extinction vector of length $A_V = 3$ mag is shown as black arrow, indicating the direction of reddening for extincted sources. The two gray dashed lines show the reddening band, plotted parallel to the extinction vector and above the main sequence. *Right:* WISE mid-infrared color-color diagram. An extinction vector of length $A_V = 5$ mag is shown as black arrow. The gray dashed line separates the groups roughly into Class II and Class III YSOs. The number of sources that fall in each class per group is given in the legend.

Figure 6 shows two infrared color-color diagrams to investigate how extinction is influencing the photometry of the two groups by using near-infrared photometry, and to investigate their evolutionary status by using mid-infrared photometry. For this analysis we use near-infrared photometry, J ($1.25 \mu\text{m}$), H ($1.65 \mu\text{m}$), and K_S ($2.16 \mu\text{m}$), from the Two Micron All-Sky Survey (2MASS; [Skrutskie et al. 2006](#)), and mid-infrared photometry, W1 ($3.4 \mu\text{m}$), W2 ($4.6 \mu\text{m}$), and W3 ($12 \mu\text{m}$), from the Wide-field Infrared Survey Explorer (WISE, AllWISE catalog; [Cutri et al. 2013](#)), retrieved from <https://irsa.ipac.caltech.edu>. To combine the 2MASS and WISE catalogs with the Gaia EDR3 astrometry we used a $1''$ cross-match radius, only keeping the closest nearest neighbor.

The left panel in Fig. 6 shows the 2MASS near-infrared color-color diagram, highlighting which sources in the two groups show significant signs of reddening, caused either by foreground extinction or by a circumstellar disk. In particular, sources above the main sequence, located within the reddening band, are thought to be dominated by foreground extinction. Only sources that pass the following quality criteria were used for the diagram:

$$\begin{aligned} j_sig, h_sig, k_sig &< 0.1 \text{ mag}, \\ j_snr, h_snr, k_snr &> 10. \end{aligned} \tag{A1}$$

$$\begin{aligned} j_sig, h_sig, k_sig &< 0.1 \text{ mag}, \\ j_snr, h_snr, k_snr &> 10. \end{aligned} \tag{A2}$$

With these cuts there are 850 and 642 sources left in Briceño-1 and OBP-near, respectively. The majority of the sources in the two groups (more than 95%) show no or very little reddening, with no significant difference between the

groups. This is expected, since the groups lie in-front of the major cloud complexes in Orion. There are few sources showing extinctions as high as about $A_V = 3$ to 8 mag, while most of these are classified as Class II YSOs based on their mid-infrared color (see below), hence the reddening could be caused by circumstellar dust. The source showing the highest reddening in Fig. 6 (2MASS J05414177-0151456 in OBP-near) is projected on top of the young embedded cluster NGC 2024 in Orion B and might rather belong to this cluster, since some contamination by other groups in our SNN selected samples can not be ruled out.

The right panel in Fig. 6 shows a WISE mid-infrared color-color diagram. To use near- to mid-infrared photometry to distinguish evolutionary classes within a young stellar population based on the infrared excess determined from the spectral energy distribution (SED) is a proofed tool since the 80s (e.g. Lada 1987; Lada et al. 2006; Großschedl et al. 2019). This allows to estimate which of the young stellar objects (YSOs) are still embedded in an envelope (Class I), are pre-main-sequence stars surrounded by a circumstellar disk (Class II), or which are pre-main-sequence stars that have already dissipated their envelope and disk and are on their way to the main-sequence (Class III). The latter class can not be strictly separated from main-sequence stars using solely mid-infrared colors, however, since we are dealing in this study with populations younger than about 10 Myr, the classification into Class III for sources with no clear infrared excess is a feasible approach. We like to note that the most massive stars of the two populations have likely already reached the main-sequence while still being young. Regarding Class I protostars, there are likely no protostars included in the Class II samples, since they tend to have redder colors beyond the borders of the displayed axes. Figure 6 only includes a rather small fraction (about 17%) of the SNN selected members, due to the inferior resolution and sensitivity of WISE compared to Gaia or 2MASS. To get reliable WISE photometry, several quality criteria have been applied to avoid erroneous photometry and contamination by extended emission, to which especially the W3 passband is susceptible to. The quality criteria are as follows:

$$\begin{aligned} w\#\text{snr} &> 10, \\ w\#\text{rchi2} &< 20, \\ w3\text{mag}_1 - w3\text{mag}_6 &< 2 \text{ mag}. \end{aligned} \tag{A3}$$

For more details on the WISE quality criteria see Großschedl et al. (2019). With these cuts there are 129 and 131 sources left in Briceño-1 and OBP-near, respectively. The Class II YSOs are separated from Class III and main-sequence stars with

$$W1 - W2 > -0.3 \cdot (W2 - W3 - 0.3) + 0.4. \tag{A4}$$

This separation is similar to class definitions in the literature based on WISE colors as discussed, for example, in Koenig & Leisawitz (2014). With this we get a Class II disk fraction of about 19% and 43% for Briceño-1 and OBP-near, respectively (only using the sources shown in Fig. 6 in the right panel). This difference in disk fraction suggests that OBP-near is at a younger evolutionary status compared to Briceño-1, in agreement with the difference in ages as obtained via isochrones in Sect. 3.